Journal of Materials Chemistry A

Accepted Manuscript

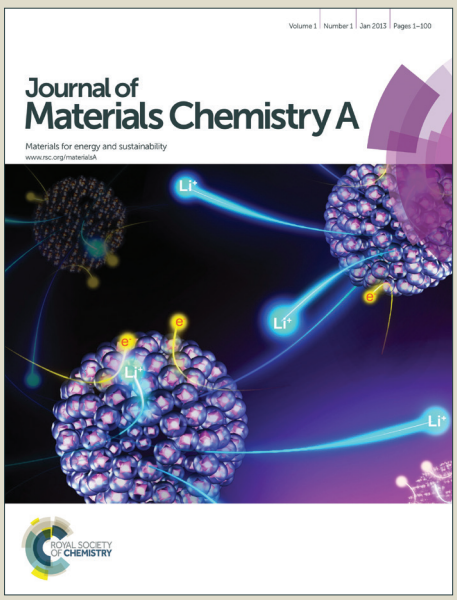

ROYAL SOCIETY OF CHEMISTRY

www.rsc.org/materialsA

Journal ofMaterials Chemistry A RSCPublishing

PAPER

Enhancement of Photocatalytic Activity for $BiPO_4$ via Phase Junction

Cite this: DOI: 10.1039/xoxxoooooox

Yanyan Zhu[a,b],Yanfang Liu[a],Yanhui Lv[a],Qiang Lin[b], Di Liu[a],Yongfa Zhu[a,*]

Received 00th April 2014,
Accepted 00th April 2014

DOI: 10.1039/x0xx00000x

www.rsc.org/

Abstract: $BiPO_4$ with phase junction were synthesized by calcinating hexagonal $BiPO_4$(HBIP) at different temperatures. The phase structures of $BiPO_4$ were gradually transformed from HBIP into monazite monoclinic $BiPO_4$ (nMBIP) and monoclinic $BiPO_4$ (mMBIP) with increasing calcination temperature. The enhancement of photocatalytic performance and photocurrent were ascribed to the formation of phase junction. nMBIP-mMBIP surface-phase junction was formed in $BiPO_4$ when HBIP was calcinated at 500 ℃, and its photocatalytic activity was 28.7 times as high as that of HBIP. Moreover, radical trapping experiments confirmed that the hole was the active species for $BiPO_4$ on the degradation of methylene blue.

Introduction

Semiconductor photocatalysis has attracted much attention owing to their superiority in environmental purification and photocatalytic hydrogen generation from water splitting in recent years[1-3]. $BiPO_4$, as a new type of oxy-acid salt photocatalyst, its electrostatic field formed by PO_4 tetrahedron on the surface promotes the separation efficiency of photo-generated charges and exhibits excellent photocatalytic activity[4, 5]. Moreover, it also possesses merits such as well stable chemical structure, exceptional optical and electronic properties, low-cost, nontoxicity and fast settlement separation speed. $BiPO_4$ nanorod and nanocrystal were synthesized by hydrothermal and solvothermal methods, and their photocatalytic activities on the degradation of methylene blue is 2.0 and 3.6 times as high as that of P25[6, 7]. To overcome the narrow absorption of $BiPO_4$, many wide absorption semiconductors such as Ag_3PO_4[8], $BiVO_4$[9, 10], C_3N_4[11], CdS[12], AgBr[13] were coupled with it. The result was found that not only the absorption range was enlarged but also the photocatalytic activity was enhanced. The photocatalytic performance of $BiPO_4$ was also further improved by adjusting surface oxygen vacancy[14, 15] and doping fluorine[16] or Ag[17, 18]. However, for the practical use of $BiPO_4$ in the environment, some problems need to be solved including complicated synthetic method, low yield, low specific surface area and so on.

Phase structure is a major factor that influences photocatalytic activity. For traditional TiO_2, the activity of anatase is better than that of rutile, but the photocatalytic activity of P25 consisted of 80% anatase and 20% rutile is superior to that of pure anatase TiO_2[19]. The correlation between the phase junction of TiO_2 and the photocatalytic activity is not fully understood. In recent years, phase junction of TiO_2[20, 21], α-β phase junction of Ga_2O_3[22] and Bi_2O_3 nanowires[23] were formed by different methods. The formation of phase junction efficiently accelerated the separation efficiency of photo-generated charges and further improved the photocatalytic performance. For $BiPO_4$, there are three main phase structures: hexagonal $BiPO_4$ (HBIP, space group: P3121), monazite monoclinic $BiPO_4$ (nMBIP, space group: P21/n) and monoclinic $BiPO_4$ (mMBIP,space group: P21/m). Among them, nMBIP has the highest photocatalytic activity because of the most distorted PO_4 tetrahedron and the largest dipole moment, and the HBIP has the lowest photocatalytic activity[7, 24-27]. Is it possible to obtain a more efficient photocatalyst by forming the phase junction of $BiPO_4$?

In this work, $BiPO_4$ with phase junction were synthesized by calcinating HBIP at different temperatures, and the enhancement of photocatalytic activity was explored. Besides, the mechanism for the improved photocatalytic performance by phase junction has been discussed.

1. Experimental Section

1.1 Chemical Reagents

Bismuth nitrate pentahydrate ($Bi(NO_3)_3\cdot5H_2O$), sodium dihydrogen phosphate dihydrate ($NaH_2PO_4\cdot2H_2O$) and ethanol were purchased from Beijing Chemical Works of China. Glycerol was purchased from Tianjin Fuchen Chemical Reagents Factory of China. Methylene blue, methyl orange and RhodamineB were purchased from Tianjin Chemical Reagent Limited Corporation of China. All chemical reagents used were analytic grade directly without further purification.

2.2 Synthesis of $BiPO_4$ with phase junction

4.85 g (10 mmol) $Bi(NO_3)_3\cdot5H_2O$ was dissolved in 900 mL 10% glycerol–H_2O mixed solution. The mixture was sonicated for 1 h until $Bi(NO_3)_3\cdot5H_2O$ was dissolved completely， and then 7.8 g (50 mmol) $NaH_2PO_4\cdot2H_2O$ was added into the solution. The white suspension was formed immediately and then stirred for 1 h. A white precipitate was obtained by centrifugation and washed with ethanol and deionized water for

three times respectively. Finally, the product was dried at 120 ℃ for 12 h and which was HBIP. $BiPO_4$ with different phase structure were prepared by calcinating HBIP at several different temperatures in the range of 350-650 ℃ for 4 h and at 500 ℃ for different times in a muffle furnace in air.

2.3 Photocatalytic Activity and Photoelectrochemical Performance

The photocatalytic activities of as-prepared $BiPO_4$ were evaluated on the degradation of methylene blue in solution under a 15 W 254 nm UV germicidal lamp and the average light intensity was 0.90 mW·cm^{-2}. 25 mg photocatalyst was added into as-prepared 50 mL 3.0×10^{-5} mol·L^{-1}methylene blue aqueous solution. Prior to UV irradiation, the suspension was ultrasonically dispersed for 0.5 h and then magnetically stirred for 1.0 h in dark to ensure the establishment of adsorption−desorption equilibrium. At each given time intervals, 3.0 mL suspension was taken and separated through centrifugation (4000 rpm, 10 min). The concentration of the methylene bluesolution was analyzed at the absorption band maximum (663 nm) using a Hitachi U-3010 UV-Vis spectrophotometer. The methods for the photocatalytic degradation of methyl orange, Rhodamine B and phenol were the same as above, but the concentration of phenol was 10.0 mg·L^{-1}. The concentration of phenol is monitored using HPLC analysis with a UV detector at 270 nm. The mobile phase was methanol and water (6:4), and the flow rate was 1.0 mL•min^{-1}.

The photocurrents and electrochemical impedance spectroscopy (EIS) were performed on CHI-660B electrochemical system (Shanghai, China) using a standard three-electrode cell with a working electrode (20 mm×45 mm , ITO/$BiPO_4$), using a standard calomel electrode (SCE) as reference electrode and a platinum wire as counter electrode. ITO/$BiPO_4$was prepared by a dip−coating method: 6 mg photocatalyst was suspended in 0.75 mL ethanol to make slurry, which was then dip−coated onto ITO glass electrode. The as−prepared electrodes were dried under ambient conditions for about 12 h and then calcinated at 120 ℃ for 5 h in air. Photoelectrochemical properties were measured with an 11 W germicidal lamp with 254 nm. Unless otherwise stated, the intensity of light at the film electrode was 1.5 mW·cm^{-2} at the wavelength of 254 nm and 0.1 mol·L^{-1} Na_2SO_4 electrolytes were used. The photoelectric responses of the photocatalysts as light on and off were measured at 0.0 V. The electrochemical impedance spectroscopy (EIS) was carried out at the open circuit potential, and a sinusoidal ac perturbation of 5 mV was applied to the electrode over the frequency range of 0.05–10^5 Hz.

2.4 Materials Characterization

The purity and crystallinity of the as-prepared sample were characterized by X-ray diffraction (XRD) on a Bruker D8-advance diffractometer using (Cu Kα=1.5418 Å) at a scan rate of 2 °·min^{-1} in the 2θ range from 10° to 60°. The high-resolution transmission electron microscope (HRTEM, JEM 2010F) was operated at an accelerating voltage of 200 kV. The Raman spectrum was measured at room temperature using HORIBAR 800 microscopic confocal Raman spectrometer in the range of 2000 cm^{-1} to 4000 cm^{-1},and the excitation light was the 514.5 nm from an Ar^+ laser with 30 mW output power. Ultraviolet−Visible diffuse reflectance spectroscopy (UV-Vis DRS) was performed on Hitachi U-3010 UV-Vis spectrophotometer, and $BaSO_4$ was used as reference sample. Thermo gravimetric analysis (TG) and differential scanning calorimetry (DSC) were carried out using a NETZSCH STA 449F3 simultaneous thermal analyzer in dry air in the range of 50-900 ℃ at a heating rate of 10 ℃·min^{-1}. Transmission electron microscopy (TEM) was recorded on a HITACHI HT7700 electron microscope at an accelerating voltage of 100 kV. Scanning electron microscopy (SEM) images were taken on a LEO1530 thermal field emission scanning electron microscope operating at an accelerating voltage of 10.0 kV. The photoluminescence (PL) emission spectra of as-prepared samples were measured on Aqualog®absorbance and 3D fluorescence scanning spectrophotometer with 150 W of 250 nm exciting light.

2. Results and Discussions

2.1 Formation of $BiPO_4$ phase junction

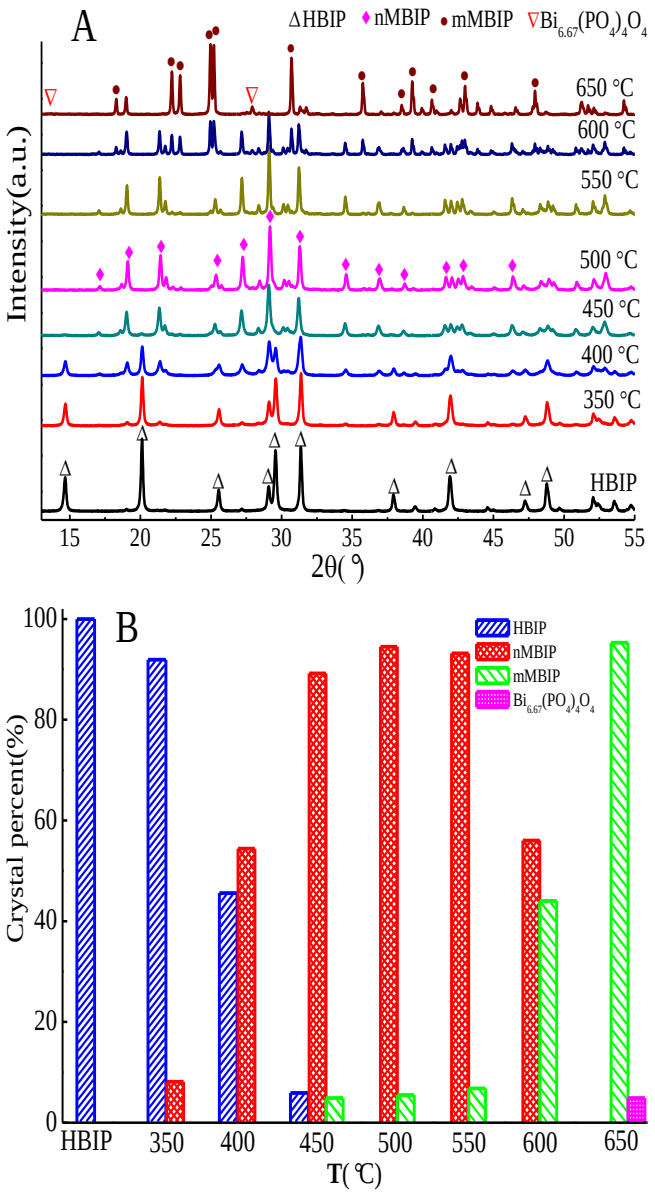

Fig.1 (A) The XRD patterns and (B) crystal compositions of $BiPO_4$ synthesized by calcinating of HBIP at different temperatures for 4.0 h

$BiPO_4$ with phase junction were synthesized by gradual phase transformation from HBIP into nMBIP and mMBIP via calcination in the range of 350-650 ℃ (Fig.1A). $BiPO_4$ lost some P atoms and O atoms when the calcination temperature was increased up to 650 ℃, which was transformed into

$Bi_{6.67}(PO_4)_4O_4$. All the diffraction peaks of precursor $BiPO_4$were indexed to the pure HBIP (P3121,JCPDS 015-0766), and no impurity peaks were observed[28]. The peaks at 19.0°, 21.4° and 27.2° emerged after 350 ℃ calcination, which were ascribed to (011), (-111) and (200) lattice plane of nMBIP (P21/n, JCPDS 089-0287), but the proportion of nMBIP was little (Fig.1A and 1B). The proportion of nMBIP was more than that of HBIP and its percentage was 54.4% at 400 ℃. The characteristic peaks of $BiPO_4$ at 18.3°, 22.2° and 37.1° belonged to (100), (110) and (200) lattice plane of mMBIP (P21/m, JCPDS077-2208) emerged upon increasing the calcination temperature up to 450 ℃[7]. At the same time, the three kinds of phase structures $BiPO_4$ (HBIP, nMBIP and mMBIP) were existed simultaneously and their percentages were 5.9%, 89.2% and 4.9% respectively. HBIP disappeared completely and the proportion of nMBIP was increased to 94.5% at 500 ℃, and its crystal compositions were almost the same as that of $BiPO_4$calcinated at 550 ℃. Calcination times hardly affected the composition of $BiPO_4$ when calcinated temperature was set at 500 ℃ (Fig.S1). mMBIP rapidly increased with further elevating the calcination temperature above 550 ℃. nMBIP completely disappeared in $BiPO_4$ calcinated at 650 ℃, which lost some P atoms and O atoms were transformed into $Bi_{6.67}(PO_4)_4O_4$. The result is similar to other semiconductor photocatalysts. TiO_2 with different phase structures was prepared by phase transformation from anatase to rutile when calcination temperatures were in the range of 500-800 ℃[20]. Ga_2O_3 and Bi_2O_3 could formed α–β phase junction by adjusting calcination and hydrothermal temperatures[22, 23].

For HBIP precursor, the 2.0% obvious weight loss occurring from 90 ℃ to 150 ℃ could be attributed to desorption of surface bound water[27], and an endothermic peak around 100 ℃ in the DSC curve consisted with that (Fig.S2). Moreover, a sharp exothermic peak situated at 550 ℃ resulted from the phase transformation of $BiPO_4$. Because the analysis of TG and DSC were processed at continuous heating-up, so the information of measurement couldn't reflect the transformation details of three kinds of $BiPO_4$ phase structure. The phase transformation of $BiPO_4$ only changed the arrangement direction of Bi and P atoms and didn't destroy relevance of phase structure and topology[29], so there wasn't weight loss when phase transformation of $BiPO_4$ occurred.

The transformation of $BiPO_4$ phase structures could be confirmed by HRTEM images (Fig.2). The lattice fringes with d-spacing of 0.442 nm, 0.349 nm and 0.307 nm were in good agreement with (101), (110) and (111) lattice planes of HBIP (JCPDS 015-0766) (Fig.2A). $BiPO_4$ calcinated at 400 ℃ only possessed (-212) and (200) lattice planes of nMBIP (JCPDS 089-0287) with d-spacing of 0.243 nm and 0.328 nm (Fig.2B). Upon further increasing calcination temperature up to 500 ℃, $BiPO_4$ mainly had (-212) lattice plane of nMBIP with d-spacing of 0.243 nm and a small quantity of (020) lattice plane (d-spacing=0.354 nm) of mMBIP (JCPDS077-2208) emerged on the edge of nMBIP (020) lattice plane (Fig.2C). It was observed that the surface-phase junction between nMBIP and mMBIP was formed. In general, the formation of phase junction was from the two kind of crystal phase with very close lattice parameter. The (-212) lattice plane of nMBIP with d-spacing of 0.243 nm and the (020) lattice plane of mMBIP with d-spacing of 0.354 nm emerged simultaneously in Fig.2C. The specific crystal plane of phase junction was formed because of lattice mismatch during the process of calcination. The lattice fringe of mMBIP (020) lattice plane wasn't very clear on the edge of nMBIP (020) lattice plane because phase transformation was occurred from nMBIP into mMBIP in the surface region. $BiPO_4$possessed (020) and (101) lattice planes of mMBIP with d-spacing of 0.354 nm and 0.320 nm with calcination temperature increasing up to 600 ℃ (Fig.2D). As can be known from XRD(Fig.1A), $BiPO_4$ calcinated at 400 ℃ was consist of HBIP and nMBIP, which calcinated at 600 ℃ was consist of nMBIP and mMBIP. At the same time, the proportions of the two different phases were almost equal. But HRTEM images only showed the nMBIP and mMBIP lattice fringes in $BiPO_4$ calcinated at 400 and 600 ℃, respectively. The results indicated that the transformation of $BiPO_4$ phase structure at elevating temperatures is from outer surface region into inner bulk region, so the HBIP and nMBIP lattice plane couldn't be observed because they were covered by nMBIP and mMBIP completely in the outer region. However, the nMBIP and mMBIP lattice fringes could be observed simultaneously in $BiPO_4$ calcinated at 500 ℃. The result indicated that surface-phase junction formed between nMBIP and mMBIP.

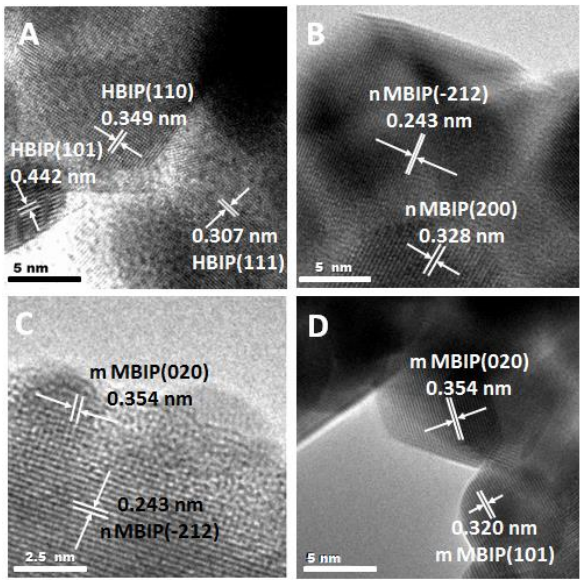

Fig.2 HRTEM images of $BiPO_4$ calcinated at different temperatures (A HBIP, B 400 ℃, C 500 ℃, D 600 ℃)

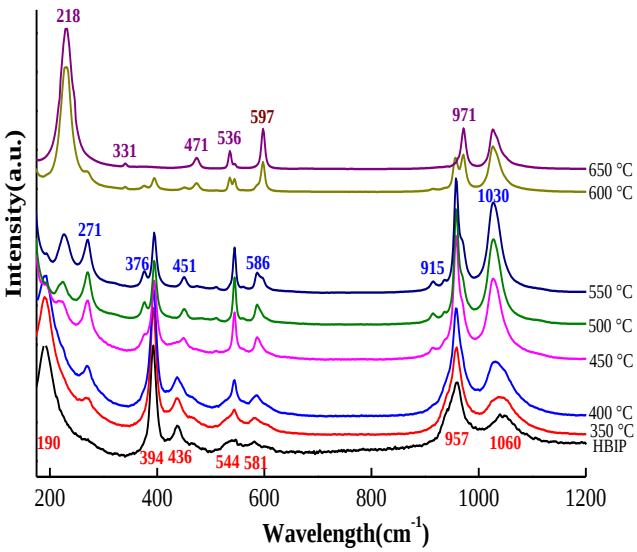

F

Fig.3 Raman spectra of HBIP and $BiPO_4$ calcinated at different temperatures for 4 h(excitation at 514.5 nm)

The three kinds of $BiPO_4$ phase structures are all constructed by building blocks of PO_4 tetrahedra and BiO_8 polyhedra, but the arrangements of polyhedral were different[5,27]. In the HBIP precursor, two intense bands at 1060 cm^{-1} and 957 cm^{-1} were ascribed to ν3 asymmetric and ν1 symmetric stretching modes of the P-O bonds in the PO_4 units respectively[27]. The bands at 581cm^{-1}, 544 cm^{-1} and 436 cm^{-1}, 394 cm^{-1} belonged to the O-P-O bending modes of ν4 and ν2 in PO_4 units. The intense band at 190 cm^{-1} may be assigned to an O-Bi-O symmetric bending mode[16,28,30]. With the calcination temperature increasing, the characteristic Raman bands of $BiPO_4$ changed significantly. When $BiPO_4$ was calcinated at 350 ℃,three new bands at 915 cm^{-1}, 376 cm^{-1} and 271 cm^{-1} belonged to ν1 symmetric stretching modes, ν2 bending modes and Bi-O stretching modes were observed, respectively.This ascribed to the characteristic Raman peaks of nMBIP gradually strengthening with the calcination temperature increasing below 550 ℃. At the same time, ν1 symmetric stretching modes showed a blue shift to 1030 cm^{-1}, ν4 and ν2 bending modes of PO_4 units showed a red shift to 586 cm^{-1} and 451 cm^{-1}[16]. Upon the calcination temperature increasing up to 600 ℃ or above, the bands positioned at 971cm^{-1}, 597cm^{-1}, 536cm^{-1}, 471 cm^{-1}, 331 cm^{-1} and the strongest band at 218 cm^{-1} was PO_4 units and Bi-O stretching modes, which were the typical Raman peaks of mMBIP.

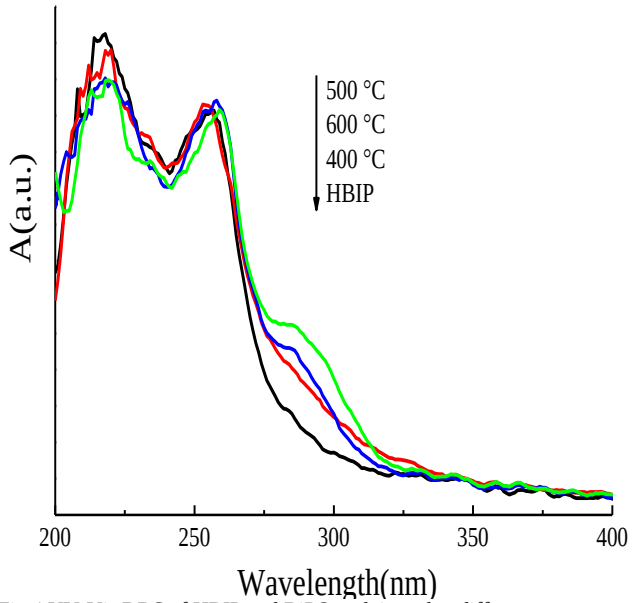

Fig.4 UV-Vis DRS of HBIP and $BiPO_4$ calcinated at different temperatures

The UV-Vis DRS of $BiPO_4$ calcinated at different temperatures were shown in Fig.4. According to the spectra, the optical absorption of HBIP started at around 325 nm and increased steeply at around 275 nm, consisted with literature[7]. Meanwhile, it was found that $BiPO_4$ after different temperatures calcinationshowed two absorption steps at about 275 nm and 330 nm. The optical band gapfor all these photocatalysts can be calculated by Tauc's plot[31].Absorption$^{1/2}$ (or absorption^{2}) versus energy, which may helpsto distinguish the direct or indirect transition of $BiPO_4$ crystalphases.From the calculated of Tauc's plot,the band gaps of HBIP and $BiPO_4$ calcinated at 400 ℃, 500 ℃ and 600 ℃ are 4.6 eV, 4.5 eV, 4.34 eV and 4.4 eV respectively as shown in Fig.S3. It may be caused by charge-transfer interaction between the two different phase structures of $BiPO_4$ with phase junction[32].The absorption maximum of HBIP and $BiPO_4$ calcinated at different temperatures appeared at about 218 nm and 258 nm, which could be assigned to the inter-band transition dominantly from the hybrid electrons of Bi^{3+} and O^{2-} rather than those of P^{5+5}.

Calcination temperature also affected morphology and particle size of $BiPO_4$.The precursor HBIP were totally composed of homogeneous rod-like particles about 500 nm in diameter and several micrometers in length. The morphologies of $BiPO_4$ formed at different calcination temperatures (in the range of 350-500 ℃)were basically the same, and their particles aggregated and became larger in size (Fig.S4 and Fig.S5). The particles of $BiPO_4$ melted and became larger and larger with calcination temperature increasing above 550 ℃[25]. High temperature calcination could also destroy the particles of other materials. For example, TiO_2 hollow spheres agglomerated into larger particles above 800 ℃[33]. The morphology of $FeTiO_3$ changed from nanofibers to submicron particles with increasing calcination temperature in the range of 600-1000 ℃[34].

3.2 Enhancement of Photocatalytic Activity via phase junction of $BiPO_4$

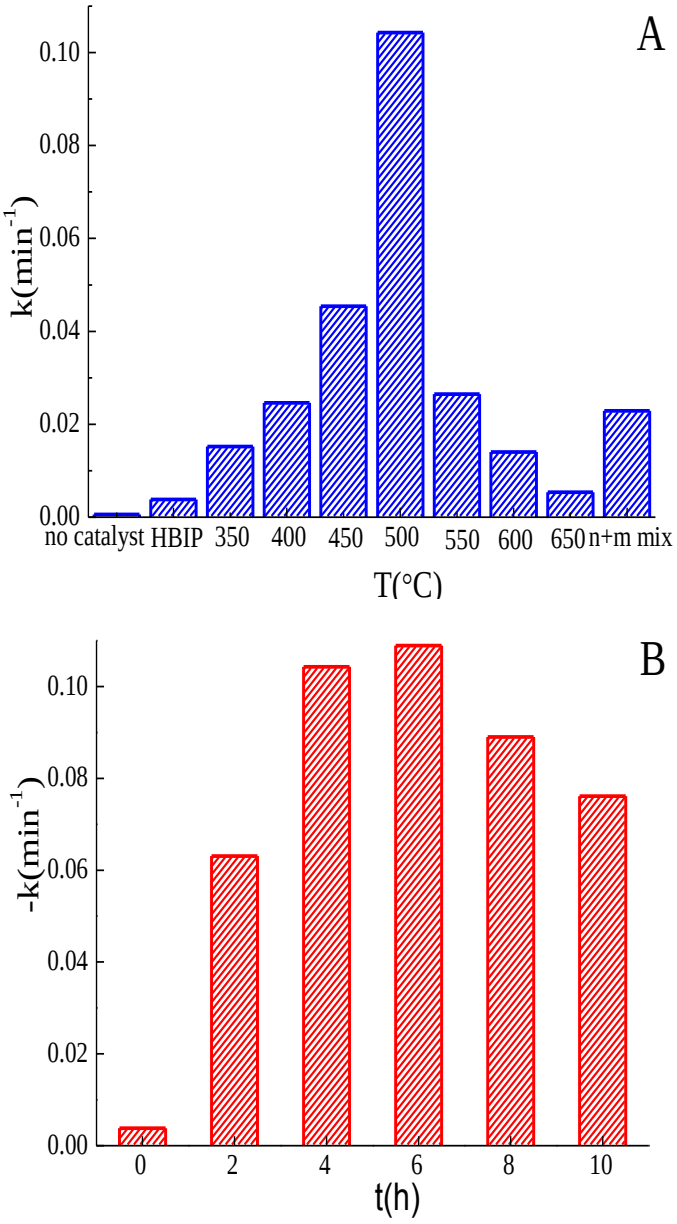

Fig.5 Apparent rate constants (k) on the photocatalytic degradation of methylene

bluefor $BiPO_4$ calcinated at (A) different temperatures for 4 h and (B) 500 ℃ for different times under 254 nm UV light irradiation

The photocatalytic degradation of methylene blue under 254 nm UV light were carried out on $BiPO_4$ with phase junction, the degradation process is fitted to pseudo-first-order kinetics. The photocatalytic performance of $BiPO_4$ firstly increased and then decreased upon increasing calcination temperature from 350 to 650 ℃(Fig.5A). Pure HBIP had very low photocatalytic activity and its apparent rate constant (k) was only 0.0038 min^{-1}, which was consistent with literature[7]. The photocatalytic activity of $BiPO_4$ gradually increased when HBIP was calcinated from 350 to 500 ℃. The maximum activity was observed when $BiPO_4$ was calcinated at 500 ℃ and the apparent rate constant k reached 0.1043min^{-1}, which was 27.4 times as high as that of HBIP. Furthermore, the photocatalytic activity of $BiPO_4$ calcinated at 500 ℃ was also much higher than that of the physical mixed sample with the same phase ratio as the former one. This may be attributed to the formation of the nMBIP and mMBIP surface-phase junction and efficient separation of photo-generated charges[20,22]. This proposition can be confirmed by the superior photocatalytic performance of $BiPO_4$ calcinated at 400 ℃ and 600 ℃ to their corresponding physical mixtures (Fig.S6).The proportion of mMBIP increased and it covered on the surface region of nMBIP when further elevating the calcination temperatures above 550 ℃. Besides, the particles of $BiPO_4$ aggregated together. The two factors might lead to the photocatalytic performance gradually decreasing. The photocatalytic activity of $BiPO_4$ calcinated at 650 ℃ was only slightly higher than that of HBIP because it was partly transformed into $Bi_{6.67}(PO_4)_4O_4$. When the calcination temperature was set at 500 ℃, the highest photocatalytic activity of $BiPO_4$ with phase junction could be obtained after calcination for 6 h. Its apparent rate constant k was 0.1089 min^{-1} and which was 28.7 times as high as that of HBIP. Parallel experiments of $BiPO_4$ calcinated at 500℃ for 6.0 h were performed. As can be seen from the result, the photocatalytic activities of these samples are almost the same, which reveals that the preparation method of $BiPO_4$ with phase junction via calcination was controllable and repeatable (Fig.S7). But when calcination time was above 6 h, the photocatalytic activities of $BiPO_4$ were decreased gradually. The apparent of $BiPO_4$ calcinated at 500 ℃ for 10 h was decreased to 0.0761 min^{-1}. Above all, the phase junction formed on the $BiPO_4$ surface could effectively enhance the photocatalytic performance.

Did the $BiPO_4$ with surface-phase junction have selectivity on the photocatalytic degradation of organic pollutants? It can be seen from Fig.6, $BiPO_4$ calcinated at 500 ℃ had much higher photocatalytic activity than HBIP on the degradation of cationic dye methyl orange, anionic dye Rhodamine B and neutral colorless reagent phenol. This indicated that $BiPO_4$ with surface-phase junction had no-selectivity and could effectively degrade different kinds of organic pollutants.

The photocatalytic activity is highly dependent on the separation efficiency of photo-generated electrons and holes[35,36]. The UV photocurrent responses of $BiPO_4$ calcinated at different temperatures for different times after deposition on ITO electrodes are provided in Fig.7. The photocurrent was stable and reversible at light-on and light-off for all samples. The photocurrent of $BiPO_4$ calcinated at 400 ℃, 500 ℃ and 600 ℃ for 4 h were 14.6 μA, 33.6 μA and 20.4 μA, but that of HBIP was only 5.3 μA. The $BiPO_4$ calcinated at 500 ℃ for 6 h showed a noticeable photocurrent, which was 43.6 μA and about 8.0 times as high as that of HBIP. The improvement of UV photocurrent indicated that the separation efficiency of photo-generated charges was improved greatly. It was in good agreement with the improvement of photocatalytic activity.

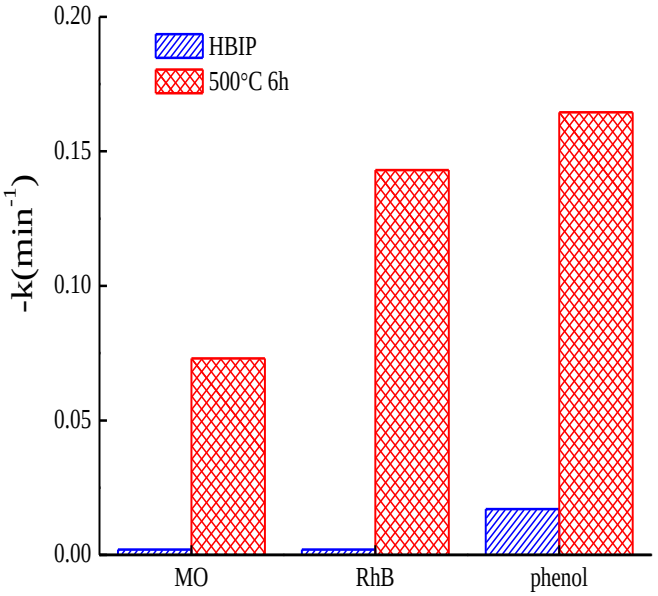

Fig.6 Photocatalytic degradation of different kinds of organic pollutants to HBIP and $BiPO_4$ calcinated at 500 ℃

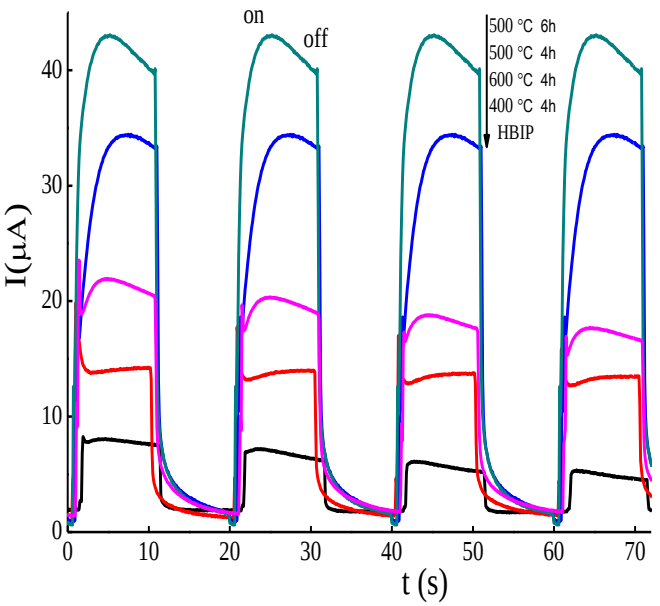

Fig.7 Photocurrents of HBIP and $BiPO_4$ calcinated on different conditions under 254 nm UV light irradiation

3.3 Mechanism for the enhanced Photocatalytic Activity via Phase Junction of $BiPO_4$

The typical EIS responses of HBIP and $BiPO_4$ calcinated under different conditions were presented in Fig. 8. In each case, there was only one arc or semicircle on the EIS images. This suggested that the transfer of surface charges was the rate-determining step in the photocatalytic reaction. The smallest arc radius on the EIS Nyquist plot indicated an efficient separation of the photo-generated electrons and holes, and vice versa [15,37,38]。 The arc radius of $BiPO_4$ with phase junction after different temperatures calcination were smaller than that of HBIP electrode in dark and under UV-light irradiation, which demonstrated that calcinated $BiPO_4$ had smaller electric resistance and higher efficiency of charge separation than HBIP. Among them, the arc radius of $BiPO_4$ calcinated at 500 ℃ for 6 h was the smallest, which further proved that nMBIP-mMBIP

surface-phase junction could effectively improve the separation and migration of photo-generated charges. Therefore, the photocatalytic activity of $BiPO_4$ calcinated at 500 ℃ was the highest.

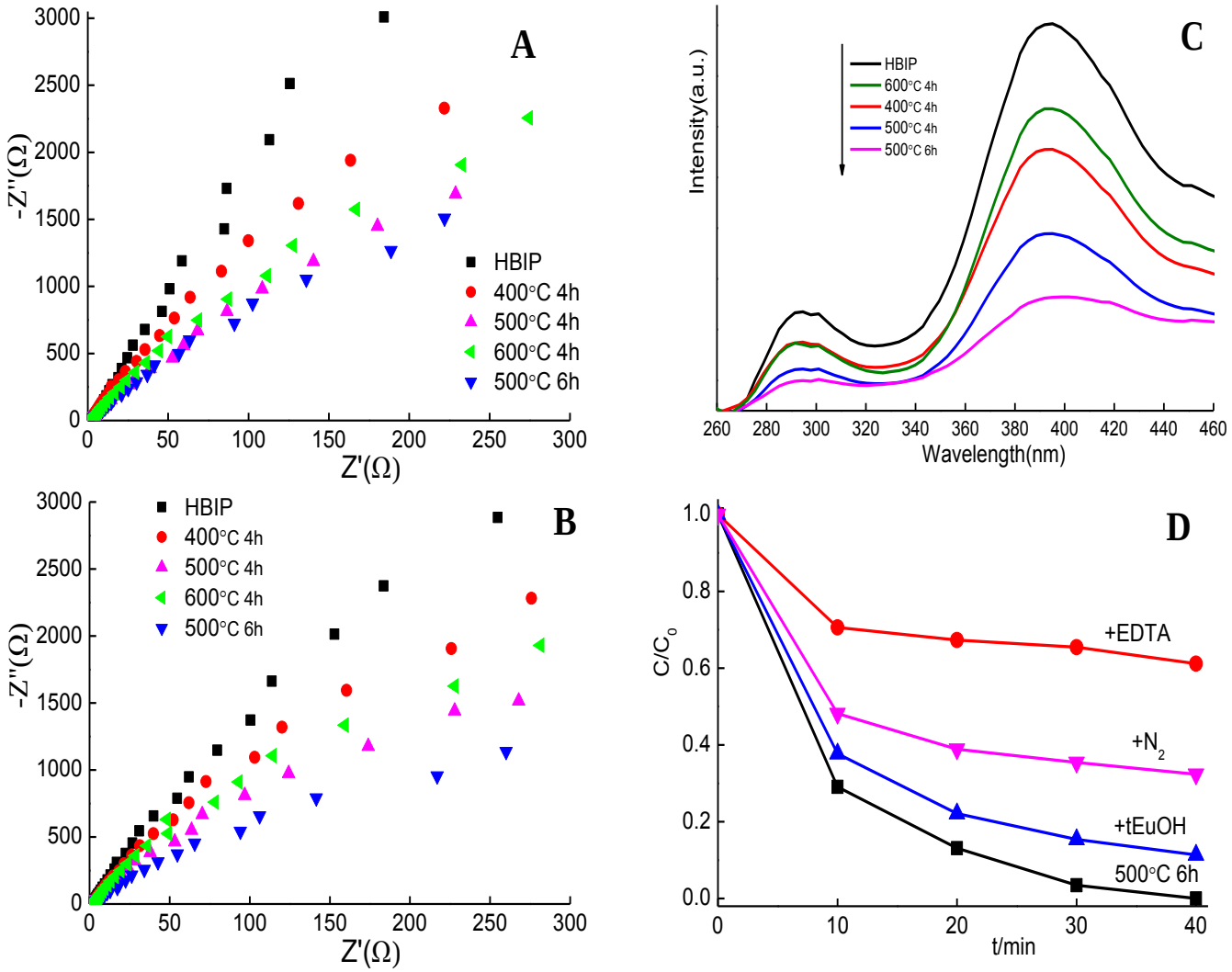

Fig.8 EIS response of $BiPO_4$ thin films electrode in dark (A) and under UV irradiation(B); (C) PL spectra of $BiPO_4$ synthesized by calcinatingHBIP under different conditions(excitation wavelength was 250 nm); (D)The plots of photocatalytic degradation of methylene blue over $BiPO_4$ calcinated at 500 ℃with the addition of hole, $\bullet O^{2-}$ and •OH radical scavenger under the 254 nm UV light irradiation

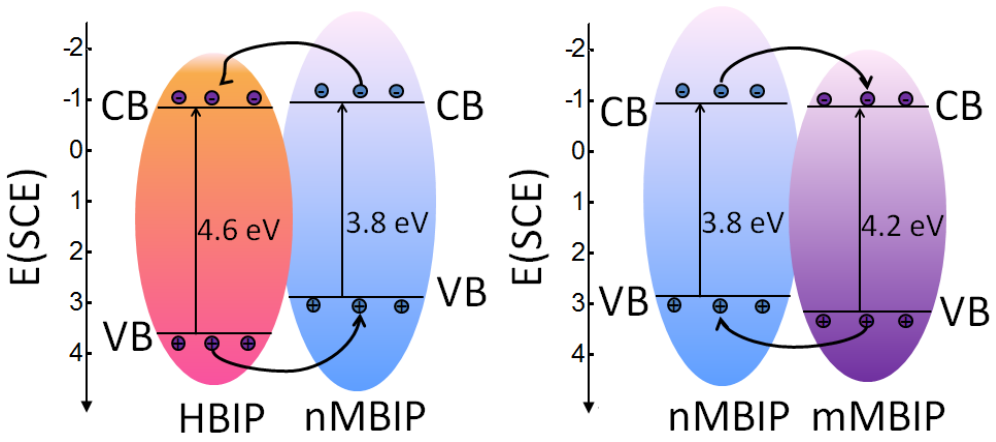

(a) HBIP-nMBIP (b) nMBIP-mMBIP

Fig.9 Schematic mechanism of charge separation and photocatalytic activity of heterojunction $BiPO_4$ photocatalyst under UV light irradiation

Journal ofMaterials Chemistry A RSCPublishing

PAPER

The PL spectra of $BiPO_4$ samples are shown in Fig.8C. It was obviously seen that the two main emission peaks were at 290 and 395 nm. As is known, the PL spectra can reflect the recombination rate of photo-generated electro-hole pairs. The emission peak intensity of HBIP was stronger than that of calcinated $BiPO_4$, which indicated that the electro-hole pair recombination rate of HBIP was faster than that of calcinated $BiPO_4$. The emission peak intensity of $BiPO_4$ calcinated at 500℃ for 6 h was the weakest. It may be caused by the formation of surface-phase junction, which improved the separation efficiency of photo-generated charges. The result was proved by EIS.

The main oxidative species could be detected by the trapping experiments of active species, using EDTA-2Na as hole scavenger, t-BuOH as hydroxyl radical scavenger and purging N_2 as $\bullet O^{2-}$ radical scavenger[36]. As shown in Fig.8D, the photocatalytic activity of $BiPO_4$ calcinated at 500 ℃ was slightly suppressed by the addition of hydroxyl radical scavenger, whereas significantly suppressed by hole scavenger. This indicated that the photo-generated holes were the major oxidative species in $BiPO_4$ calcinated at500 ℃ on the degradation of methylene blue.

A schematic for electron–hole separation and transfer at the heterojunction $BiPO_4$ photocatalyst interface is shown in Fig. 9. HBIP, nMBIP and mMBIP were all excited under 250 nm UV light irradiationand produced the photo-generated electron-hole pairs. The CB of nMBIP was the minimum, its photo-generated electrons would transfer to the CB of HBIP and mMBIP. At the same time, the VB of HBIP and mMBIP are all greater than nMBIP, their photo-generated holes would transfer to the VB of nMBIP. This made photo-generated charges separation more efficient and restrained the recombination possibility of photo-generated electron-hole, and further improved the photocatalytic performance.

Conclusions

$BiPO_4$ with phase junction were synthesized by calcinating HBIP at different temperatures. The enhancements of photocatalytic performance and photocurrent have been shown due to the efficient separation and transfer of photo-generated charges across the phase junction of $BiPO_4$. The nMBIP-mMBIP phase junction was formed on the surface region of $BiPO_4$ after calcination at 500 ℃ and it possessedthe highest photocatalytic performance. Thus, simultaneous exposure of nMBIP and mMBIP phase in the outer region is crucial for the separation of photo-generated charges. An effective method to synthesize the higher active photocatalyst was obtained via the formation of surface-phase junction.

Acknowledgements

This work was partly supported by National Basic ResearchProgram of China (2013CB632403), NationalHigh Technology Research and Development Program ofChina (2012AA062701) and Chinese National ScienceFoundation (21373121).

Notes

[a] Department of Chemistry, Tsinghua University, Beijing 100084, PR China;
b Institute of Aeronautical Meteorology and Chemical Defence, Beijing 100085, P. R. China.

Electronic Supplementary Information (ESI) available: the XRD of $BiPO_4$ calcinated at 500 ℃ for different times, TG and DSC of precursor HBIP, band gap of calculation, SEM and TEM images. This material is available free of charge by DOI: 10.1039/b000000x/

Corresponding Author:
*Fax: (+86)10-6278-7601. Tel.: (+86)10-6278-3586. E-mail: zhuyf@tsinghua.edu.cn.

References

1. J. Cao, B. Luo, H. Lin and S. Chen, *Journal of Molecular Catalysis A: Chemical*, 2011, **344**, 138-144.
2. W. Liu, M. Wang, C. Xu, S. Chen and X. Fu, *Journal of Molecular Catalysis A: Chemical*, 2013, **368-369**, 9-15.
3. T. Puangpetch, T. Sreethawong, S. Yoshikawa and S. Chavadej, *Journal of Molecular Catalysis A: Chemical*, 2009, **312**, 97-106.
4. C. Pan and Y. Zhu, *Environmental Science & Technology*, 2010, **44**, 5570-5574.
5. Y. Wang, L. Li, J. Zheng, X. Huang and G. Li, *Chemical Research in Chinese Universities*, 2013, **29**, 556-562.
6. C. Pan and Y. Zhu, *Journal Of Materials Chemistry*, 2011, **21**, 4235-4241.
7. C. Pan, D. Li, X. Ma, Y. Chen and Y. Zhu, *Catalysis Science & Technology*, 2011, **1**, 1399-1405.
8. H. Lin, H. Ye, B. Xu, J. Cao and S. Chen, *Catalysis Communications*, 2013, **37**, 55-59.
9. S. Wu, H. Zheng, Y. Lian and Y. Wu, *Materials Research Bulletin*, 2013, **48**, 2901-2907.
10. H. Lin, H. Ye, S. Chen and Y. Chen, *RSC Advances*, 2014, **4**, 10968-10974.
11. C. Pan, J. Xu, Y. Wang, D. Li and Y. Zhu, *Advanced Functional Materials*, 2012, **22**, 1518-1524.
12. T. Lv, L. Pan, X. Liu and Z. Sun, *Rsc Advances*, 2012, **2**, 12706-12709.
13. H. Xu, Y. Xu, H. Li, J. Xia, J. Xiong, S. Yin, C. Huang and H. Wan, *Dalton transactions*, 2012, **41**, 3387-3394.
14. Y. Lv, Y. Zhu and Y. Zhu, *The Journal of Physical Chemistry C*, 2013, **117**, 18520-18528.
15. Y. Lv, Y. Liu, Y. Zhu and Y. Zhu, *Journal of Materials Chemistry A*, 2014, **2**, 1174-1182.
16. Y. Liu, Y. Lv, Y. Zhu, D. Liu, R. Zong and Y. Zhu, *Applied Catalysis B: Environmental*, 2014, **147**, 851-857.

17. Y. Zhang, H. Fan, M. Li and H. Tian, *Dalton transactions*, 2013, **42**, 13172-13178.
18. M. H. Fulekar, A. Singh, D. P. Dutta, M. Roy, A. Ballal and A. K. Tyagi, *RSC Advances*, 2014, **4**, 10097-10107.
19. J. Zhu, W. Zheng, B. He, J. Zhang and M. Anpo, *Journal of Molecular Catalysis A: Chemical*, 2004, **216**, 35-43.
20. J. Zhang, Q. Xu, Z. Feng, M. Li and C. Li, *Angewandte Chemie*, 2008, **47**, 1766-1769.
21. T. Ozawa, M. Iwasaki, H. Tada, T. Akita, K. Tanaka and S. Ito, *Journal of colloid and interface science*, 2005, **281**, 510-513.
22.X. Wang, Q. Xu, M. Li, S. Shen, X. Wang, Y. Wang, Z. Feng, J. Shi, H. Han and C. Li, *Angewandte Chemie*, 2012, **51**, 13089-13092.
23. J. Hou, C. Yang, Z. Wang, W. Zhou, S. Jiao and H. Zhu, *Applied Catalysis B: Environmental*, 2013, **142-143**, 504-511.
24. Y.-F. Liu, X.-G. Ma, X. Yi and Y.-F. Zhu, *Acta Physico-Chimica Sinica*, 2012, **28**, 654-660.
25. S. N. Achary, D. Errandonea, A. Munoz, P. Rodriguez-Hernandez, F. J. Manjon, P. S. Krishna, S. J. Patwe, V. Grover and A. K. Tyagi, *Dalton transactions*, 2013, **42**, 14999-15015.
26. M. Zhao, L. Li, L. Yang, J. Zheng and G. Li, *CrystEngComm*, 2013, **15**, 609-615.
27. Y. Zhu, Y. Liu, Y. Lu, H. Wang, Q. Ling and Y. Zhu, *Acta Physico-Chimica Sinica*, 2013, **29**, 576-584.
28. G. Li, Y. Ding, Y. Zhang, Z. Lu, H. Sun and R. Chen, *Journal of colloid and interface science*, 2011, **363**, 497-503.
29. R. C. L. MOONEY-SLATER, *Zeitschrift fUr Kristallographie, Bd*, 1962, **117**, 371-385.
30. J. Geng, W. H. Hou, Y. N. Lv, J. J. Zhu and H. Y. Chen, *Inorganic Chemistry*, 2005, **44**, 8503-8509.
31. Z. Khan, M. Khannam, N. Vinothkumar, M. De and M. Qureshi, *Journal of Materials Chemistry*, 2012, **22**, 12090-12095.
32. K. Liu, Y. Yao, Y. Liu, C. Wang, Z. Li and X. Zhang, *Langmuir : the ACS journal of surfaces and colloids*, 2012, **28**, 10697-10702.
33. H. L. Shen, H. H. Hu, D. Y. Liang, H. L. Meng, P. G. Li, W. H. Tang and C. Cui, *Journal Of Alloys And Compounds*, 2012, **542**, 32-36.
34. A. Simpraditpan, T. Wirunmongkol, S. Pavasupree and W. Pecharapa, *Materials Research Bulletin*, 2013, **48**, 3211-3217.
35. Y. Wang, R. Shi, J. Lin and Y. Zhu, *Energy & Environmental Science*, 2011, **4**, 2922-2929.
36. Y. Lv, C. Pan, X. Ma, R. Zong, X. Bai and Y. Zhu, *Applied Catalysis B: Environmental*, 2013, **138-139**, 26-32.
37. L. Zhang, Y. Wang, T. Xu, S. Zhu and Y. Zhu, *Journal of Molecular Catalysis A: Chemical*, 2010, **331**, 7-14.
38. R. Shi, G. Huang, J. Lin and Y. Zhu, *Journal Of Physical Chemistry C*, 2009, **113**, 19633-19638.

Graphical Abstract

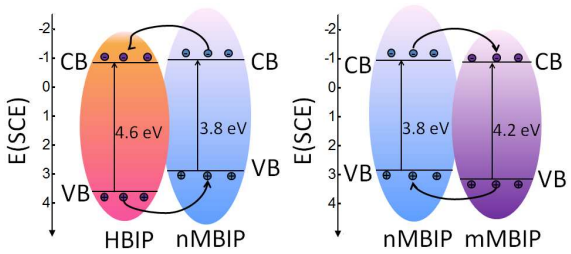

Photo-generated charges of $BiPO_4$ with phase junction could be separated and transfered quickly, which enhanced photocatalytic performance.